CT撮影

機種：**GE LightSpeed VCT (64列)**

撮影条件：120kV　スライス厚0.625mm

　中間位　約150mA　　その他の肢位は電流を1/3~半減し撮影

撮影肢位：仰臥位にて中間位、左右回旋位、前後屈位の5ポジション

X線被曝量：6-14mGy, 700-1200DLP

（医療被曝ガイドラインで定められた20mSv未満をみたす。）

大学倫理委員会承認済

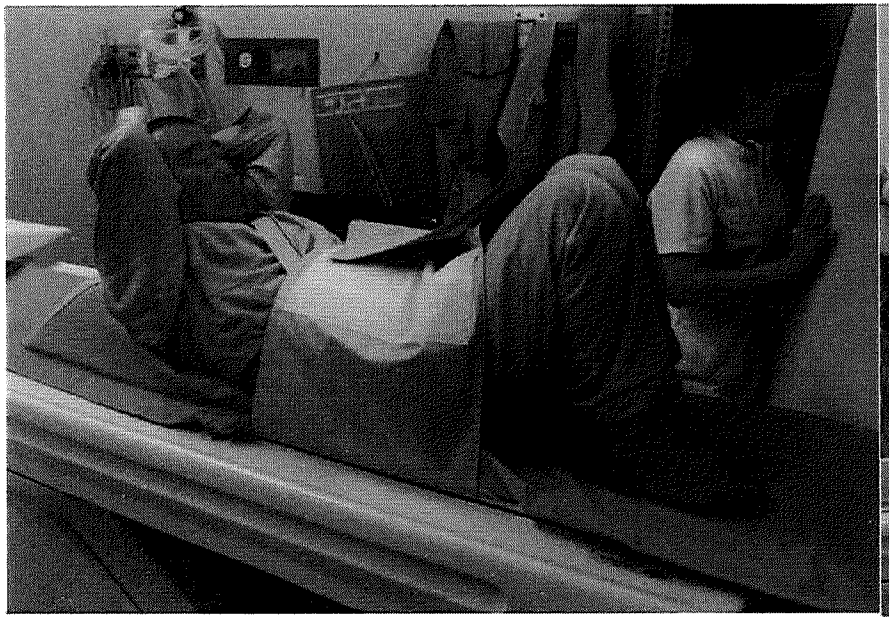

前屈位

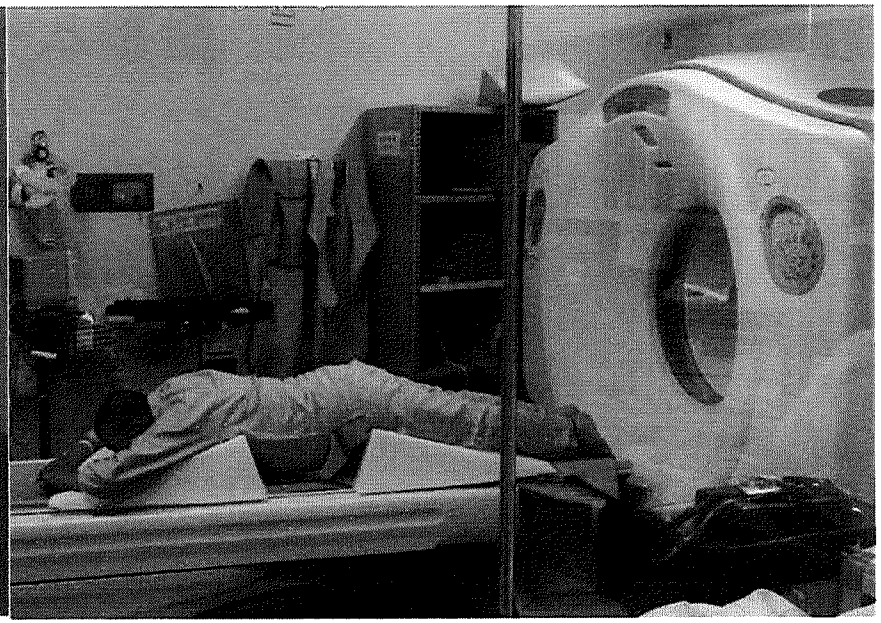

後屈位

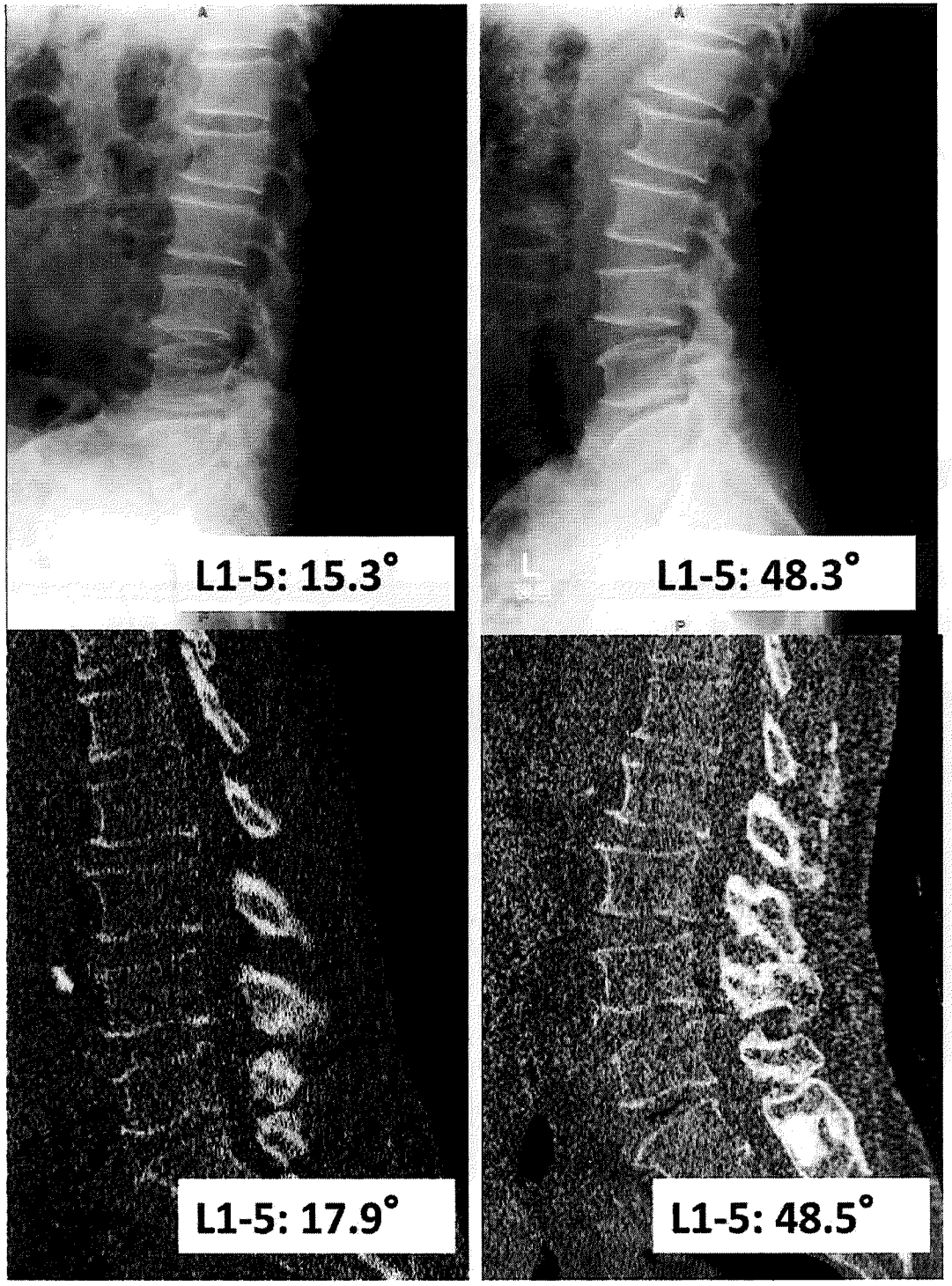

ROM
機能X-p v.s. CT

前後屈レントゲン：
ROM_{L1-5}=33°

CT
ROM_{L1-5}=30.6°

精度検定（MRIでの精度）
- Rotational error
  - axial rotation 0.43°
  - lateral bending 0.31°
  - flexion-extension 0.24°
- Translation error
  - lateral 0.41mm
  - anterior posterior 0.51mm
  - supero inferior 0.52mm

撮影手法の限界

仰臥位ベース

ガントリーの制約を強く受け、
前屈可動域を稼ぐのにコツを要する.

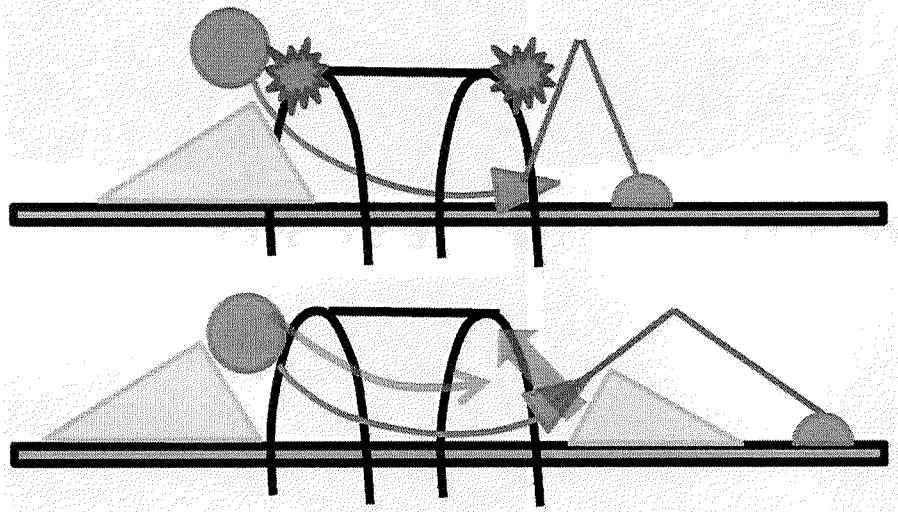

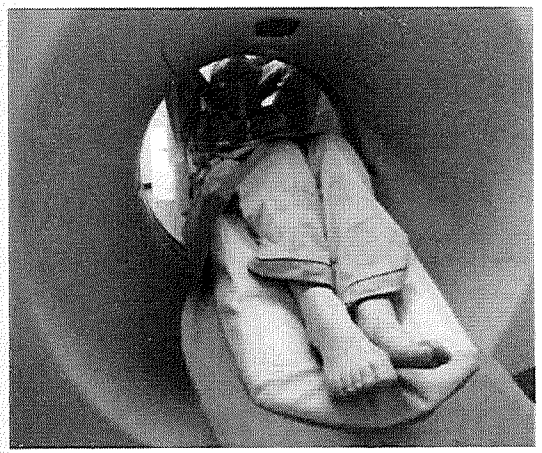

現状では安定した最大前屈可動域は得られていない.

装具改良を検討中である.

側臥位ベース

前後屈はしっかりとれるが側屈、回旋カップリングが混ざってしまう.

有効撮影症例：10例

	疾患	撮影日
3	変性側弯+L5分離辷り	H21.9.14
4	L4変性すべり	H21.9.24
5	L5/S PSF後	H21.10.1
6	L4変性すべり	H21.10.15
7	変性側弯+L4変性すべり	H21.11.2
8	L4変性すべり	H21.11.16
9	L5変性すべり	H21.12.14
10	L5分離辷り	H21.12.16
11	L4分離辷り	H21.1.4
12	L5分離辷り	H22.1.7

→画像から**大きな異常運動が予想された3症例**を解析

61y/o, M：L4変性辷り

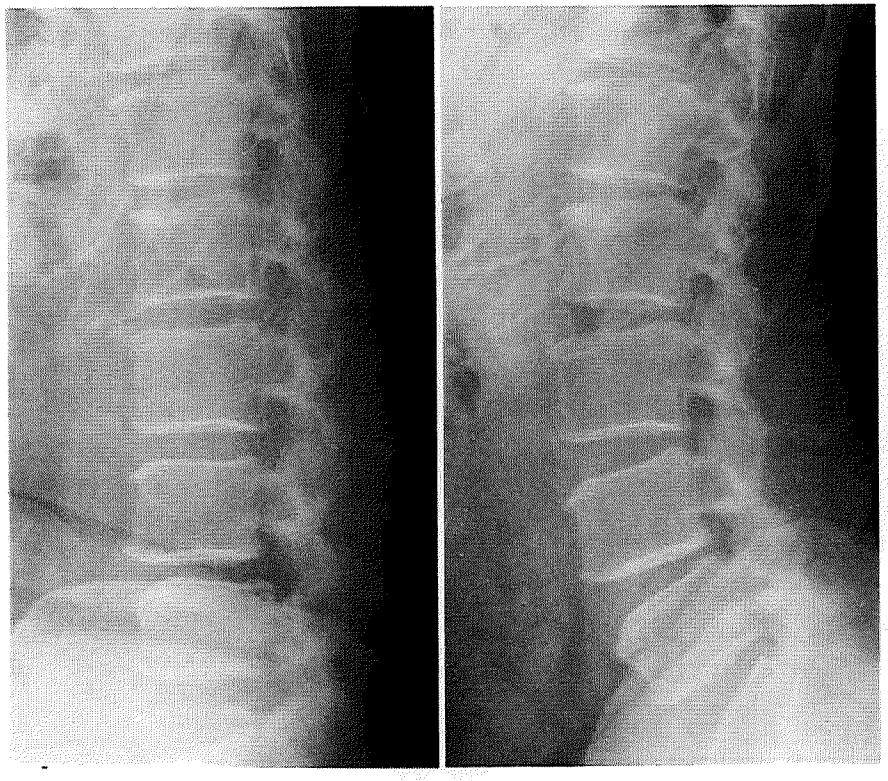

前屈位　　後屈位

L4/5 FSU

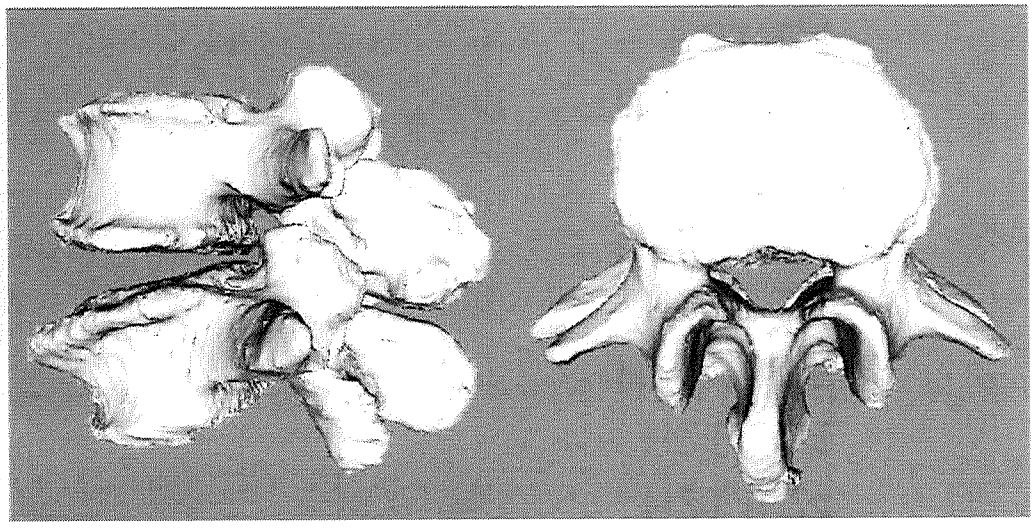

	angulation	translation
右回旋	6.2°	
左回旋	6.2°	
前屈	9.6°	前方へ1.0mm
後屈	2.4°	前方へ0.7mm

67y/o, F：L4変性辷り

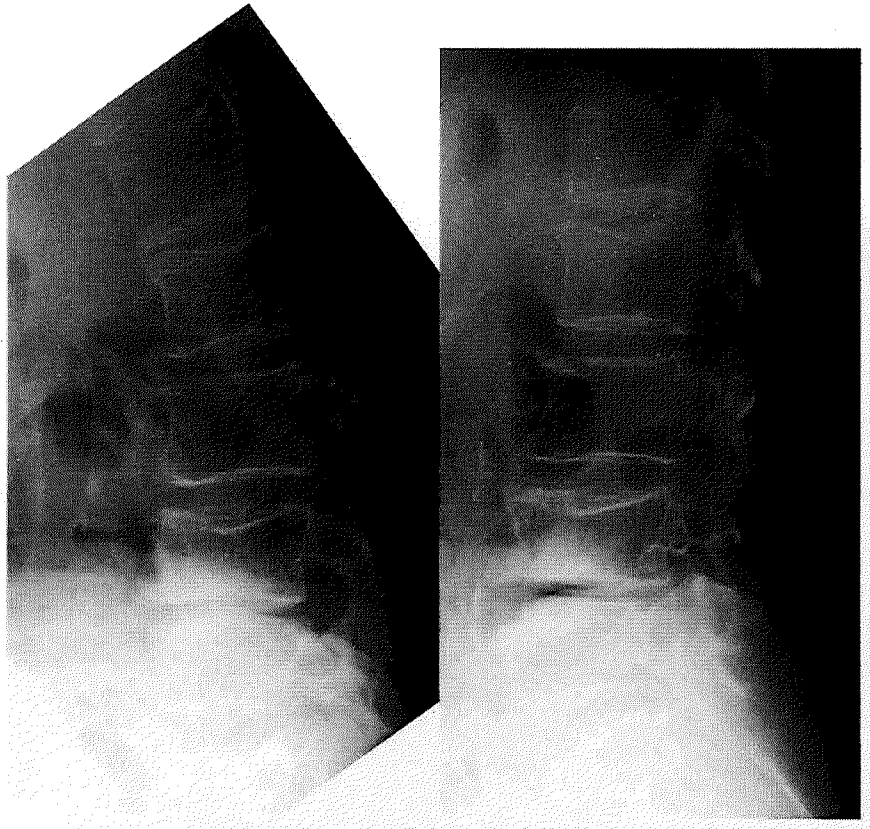

前屈位　　後屈位

L4/5 FSU

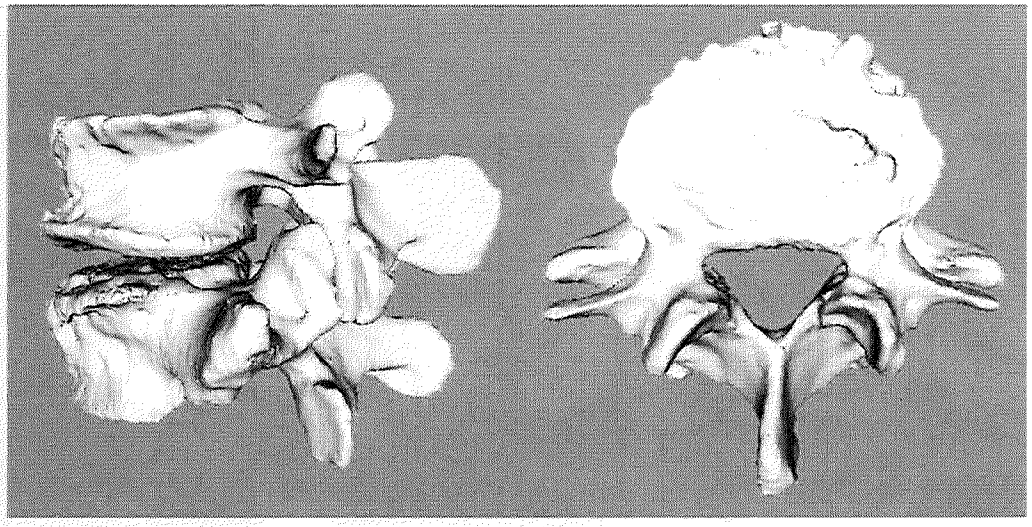

	angulation	translation
右回旋	2.7°	
左回旋	5.3°	
前屈	6.9°	後方へ0.5mm
後屈		

81y/o, F：L5分離辷り

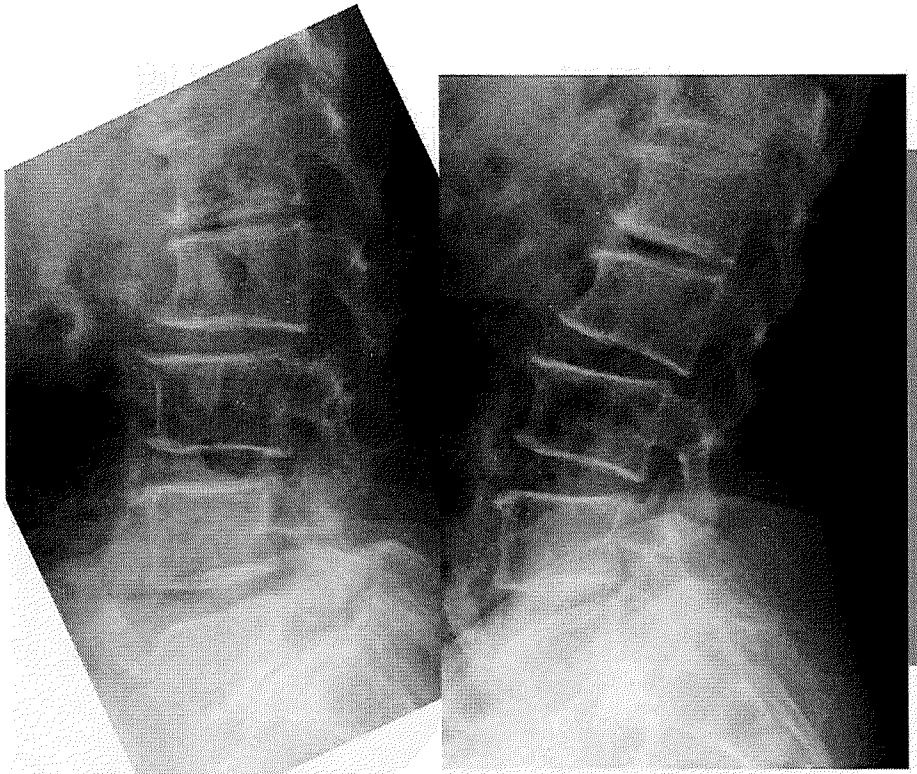

前屈位　　後屈位

L5/S FSU

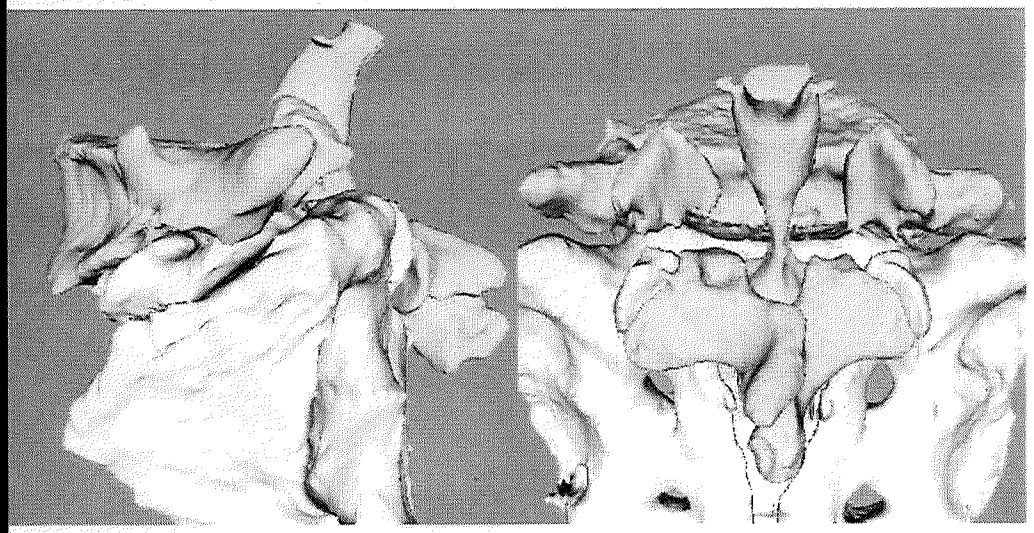

	angulation	translation
前屈	5.8°	前方へ1.5mm
後屈	-1.7°	前方へ0.8mm

仙腸関節の動き

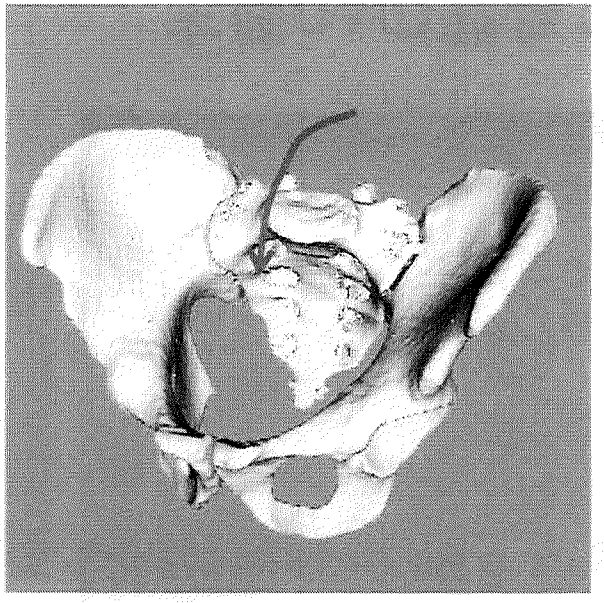

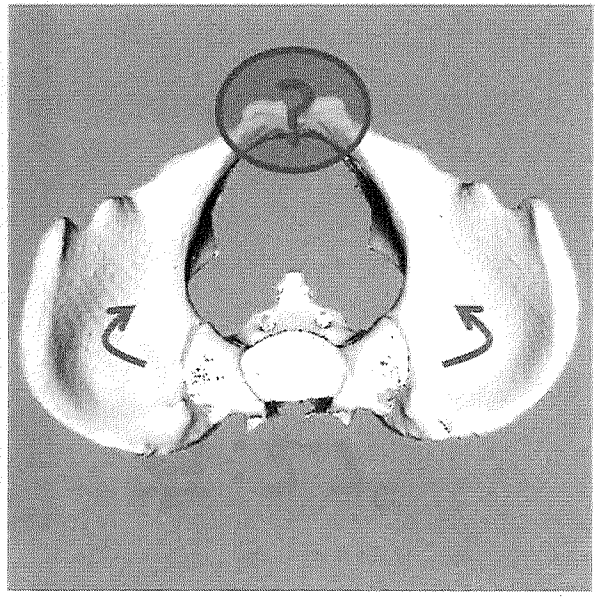

腰椎前屈時、
・仙骨も腸骨に対して前屈
・両腸骨は内旋

Screw Axis

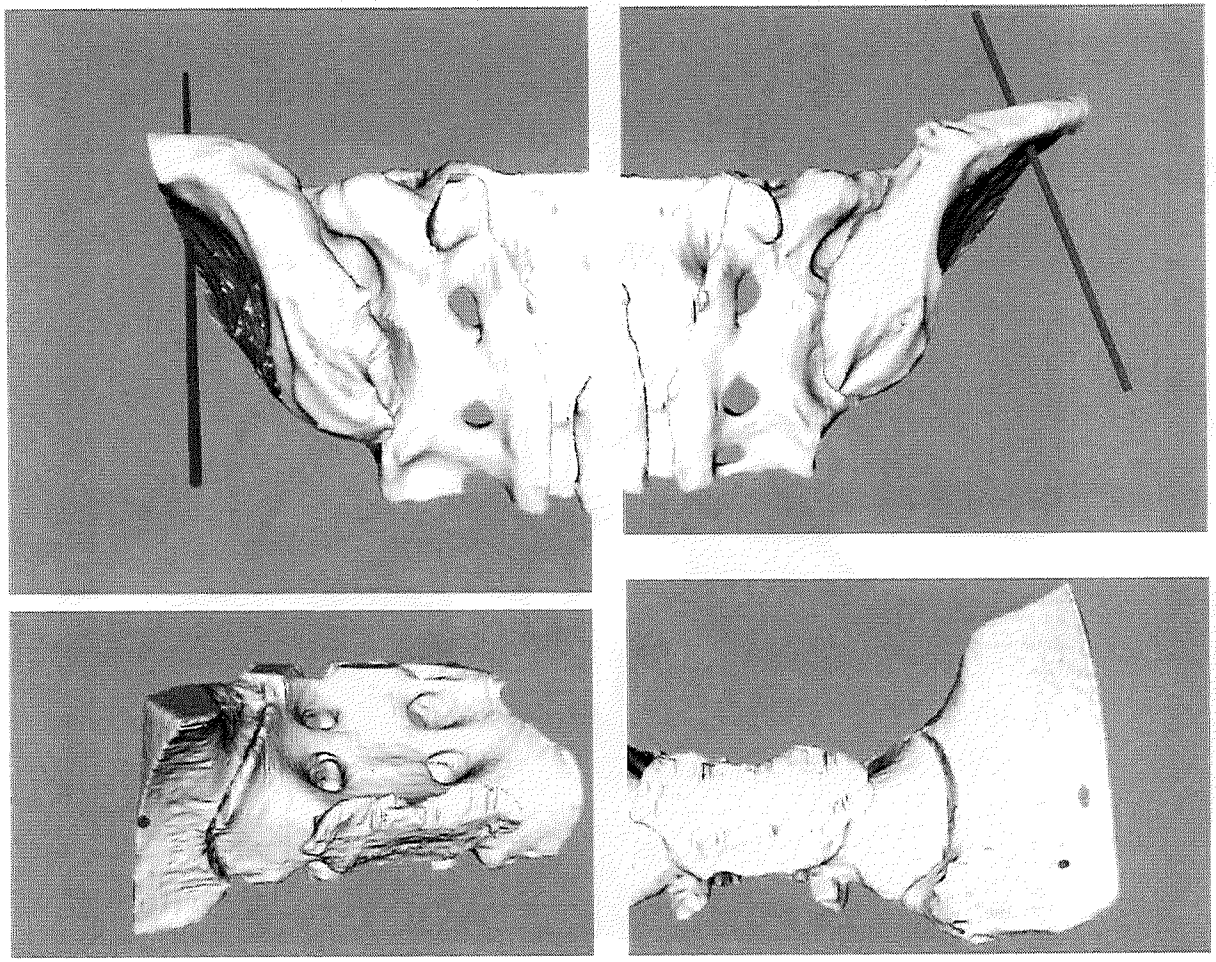

右：2.7°
左：1.4°

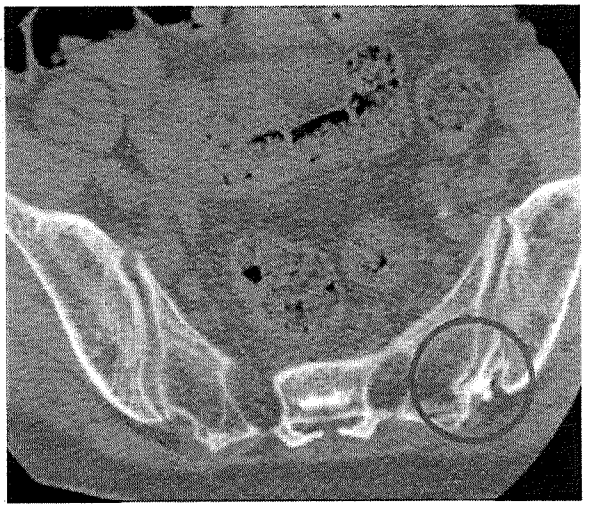

左側OAの関与？

III. 研究成果の刊行に関する一覧表

研究成果の刊行に関する一覧表

雑誌

発表者氏名	論文タイトル名	発表誌名	巻号	ページ	出版年
Takagi T, Nakamura M, Yamada M, Hikishima K, Momoshima S, Fujiyoshi K, Okano JH, Toyama Y, Okano H.	Visualizing for Peripheral Nerve Degeneration and Regeneration: Monitoring with Diffusion Tensor Tractography.	Neuroimage	44	884-892	2009
Ogawa D, Okada Y, Nakamura M, Shimazaki T, Tamiya T, Okano H	Evaluation of human fetal neural stem/progenitor cells as cell sources for cell replacement therapy for neurological disorders: their property change after long in vitro maintenance and long-term tumorigenicity in vivo.	J Neurosci Res	87	855-864	2009
Yaguchi M, Tabuse M, Ohta S, Ohkusu TK, Takeuchi T, Yamane J, Katoh H, Nakamura M, Matsuzaki Y, Yamada M, Itoh T, Toyama Y, Okano H, Toda M.	Transplantation of dendritic cells promotes functional recovery from spinal cord injury in common marmoset.	Neurosci Res	65	384-392	2009
Kumagai G, Okada Y. Yamane J, Nagoshi N, Kitamura K, Mukaino M, Tsuji O,Fujiyoshi K, Katoh H, Okada S, Shibata S, Matsuzaki Y, Toh S, Toyama Y, Nakamura M, Okano H.	Roles of ES Cell-Derived Gliogenic Neural Stem/ Progenitor Cells in Functional Recovery after Spinal Cord Injury.	PLoS ONE	4(11)	E7706	2009

Yamane J, Nakamura M, Iwanami A, Sakaguchi M, Kato h H, Yamada M, Momoshima S, Miyao S, Ishii K, Tamaoki N, Nomura T, Okano HJ, Kanemura Y, Toyama Y, Okano H.	Transplantation of Galectin-1-Expressing Human Neural Stem Cells into the Injured Spinal Cord of Adult Common Marmosets.	J Neurosci Res	88	1394-1405	2009
Okada S, Nakamra M, Saiwai H, Kumamaru H, Toyama Y, Iwamoto Y, Okano H.	Physiological signinficance of astrogliosis after CNS injury.	Inflammation and Regeneration	29	35-39	2009
Nagoshi N, Shibata S, Nakamura M, Matsuzaki Y, Toyama Y, Okano H.	Neural crest-derived stem cells display a wide variety ofcharacteristics.	Journal of Cellular Biochemistry	107	1046-1052	2009
Nakamura M, Nagoshi N, Fujiyoshi K, Kaneko S, Toyama Y, Okano H.	Regenerative medicine for spinal cord injury - Current Status and Open Issues -	Inflammation and regeneration	29	198-203	2009
金子慎二郎、中村雅也、戸山芳昭、岡野栄之	脊髄損傷後の軸索再生制御機構の解明と軸索再生促進へのストラテジー	慶應医学	85	191-195	2009
藤吉兼浩、辻収彦、松本守雄、千葉一裕、戸山芳昭、中村雅也	脊髄領域における拡散テンソルtractography	脊椎脊髄	23	315-323	2010
牛田享宏、末富勝敏、下和弘、大須賀友晃、新井健一、池本竜則	慢性痛の疼痛情報認知機構いた	ペインクリニック	30	905-913	2010
池本竜則、牛田享宏、谷俊一、上野雄文	脊髄での機能的MRI画像の試み	脳波・筋電図の臨床	52	207-2122	2010
Kobayashi Y, Kurata J, Sekiguchi M, Kokubun M, Akaishizawa T, Chiba Y, Konno S, Kikuchi S.	Augmented cerebral activation by lumbar mechanical stimulus in chronic low back pain patients. An fMRI study	Spine	22	2341-2436	2009

岩崎幹季	特発性頸椎後弯症の病態と予後予測	脊椎脊髄	22	539-543	2009
梶浦一朗、森口悠、岩崎幹季、他	腰部脊柱管狭窄症の術前評価にミエログラフィーは必要か？－MRIとの比較－	J Spine Res	1	198	2010
大島和也、和田英路、岩崎幹季、他	頸椎の新しい評価基準（JOACMEQ）とJOAスコアの比較	脊椎脊髄	23	201-205	2010

IV. 研究成果の刊行物・別刷

NeuroImage 44 (2009) 884–892

Contents lists available at ScienceDirect

NeuroImage

journal homepage: www.elsevier.com/locate/ynimg

Visualization of peripheral nerve degeneration and regeneration: Monitoring with diffusion tensor tractography☆

Takehiko Takagi [a,b], Masaya Nakamura [a], Masayuki Yamada [e,f], Keigo Hikishima [d,e], Suketaka Momoshima [c], Kanehiro Fujiyoshi [a,b], Shinsuke Shibata [b], Hirotaka James Okano [b], Yoshiaki Toyama [a], Hideyuki Okano [b,*]

[a] Department of Orthopaedic Surgery, Keio University School of Medicine, 35 Shinanomachi, Shinjuku-ku, Tokyo 160-8582, Japan
[b] Department of Physiology, Keio University School of Medicine, 35 Shinanomachi, Shinjuku-ku, Tokyo 160-8582, Japan
[c] Department of Diagnostic Radiology, Keio University School of Medicine, 35 Shinanomachi, Shinjuku-ku, Tokyo 160-8582, Japan
[d] Center for Integrated Medical Research, Keio University, 35 Shinanomachi, Shinjuku-ku, Tokyo 160-8582, Japan
[e] Central Institute for Experimental Animals, 1430 Nogawa, Miyamae-ku, Kawasaki, Kanagawa, 216-0001, Japan
[f] Faculty of Radiological Technology, Fujita Health University School of Health Sciences, 1-98 Dengakugakubo, Kutsukake-cho, Toyoake-shi, Aichi 470-1192, Japan

ARTICLE INFO

Article history:
Received 1 July 2008
Revised 15 September 2008
Accepted 17 September 2008
Available online 2 October 2008

Keywords:
Diffusion tensor imaging
Diffusion tensor tractography
Peripheral nerve injury
Fractional anisotropy
Wallerian degeneration
Magnetic resonance imaging

ABSTRACT

We applied diffusion tensor tractography (DTT), a recently developed MRI technique that reveals the microstructures of tissues based on its ability to monitor the random movements of water molecules, to the visualization of peripheral nerves after injury. The rat sciatic nerve was subjected to contusive injury, and the data obtained from diffusion tensor imaging (DTI) were used to determine the tracks of nerve fibers (DTT). The DTT images obtained using the fractional anisotropy (FA) threshold value of 0.4 clearly revealed the recovery process of the contused nerves. Immediately after the injury, fiber tracking from the designated proximal site could not be continued beyond the lesion epicenter, but the intensity improved thereafter, returning to its pre-injury level by 3 weeks later. We compared the FA value, a parameter computed from the DTT data, with the results of histological and functional examinations of the injured nerves, during recovery. The FA values of the peripheral nerves were more strongly correlated with axon-related (axon density and diameter) than with myelin-related (myelin density and thickness) parameters, supporting the theories that axonal membranes play a major role in anisotropic water diffusion and that myelination can modulate the degree of anisotropy. Moreover, restoration of the FA value at the lesion epicenter was strongly correlated with parameters of motor and sensory functional recovery. These correlations of the FA values with both the histological and functional changes demonstrate the potential usefulness of DTT for evaluating clinical events associated with Wallerian degeneration and the regeneration of peripheral nerves.

Introduction

MRI, an indispensable tool in the diagnosis of central nervous system disorders, has rarely been applied to diseases of the peripheral nervous system, because it is difficult to delineate peripheral nerves on account of their poor contrast with the surrounding tissues. The standard repertoire for diagnosing peripheral nerve disorders includes clinical and electrophysiological examinations, supplemented by more invasive procedures.

For the differential diagnosis of peripheral nerve lesions, the visualization of peripheral nerves using MRI has been attempted using special techniques such as MR neurography (Filler et al., 2004; Howe et al., 1992). However, the interpretation of the images obtained by MR neurography is based on visual inspection, and is therefore qualitative and subjective. Furthermore, since MR neurography cannot image continuous nerve fibers over their entire length, it is not considered useful for examining the growth of regenerating peripheral nerves. To visualize nerve fibers in MRI, a contrast agent such as superparamagnetic iron oxide (SPIO) (Bendszus and Stoll, 2003) or gadofluorine M (Bendszus et al., 2005; Wessig et al., 2008) can be injected, but this is invasive. The difficulty in visualizing axons makes these methods impractical for evaluating peripheral nerve injury in the present clinical scenario.

To overcome these shortcomings, here we applied diffusion tensor imaging (DTI), a non-invasive method that reveals the microstructure of tissues on the basis of its ability to monitor the random movements of water molecules (Basser et al., 1994). Diffusion tensor tractography (DTT) refers to the analysis and reconstruction of the data obtained by DTI, by which the orientation of nerve fibers can be followed to trace specific neural pathways, such as that of the corticospinal tract in the brain or the spinal cord (Conturo et al., 1999; Fujiyoshi et al., 2007; Mori and Zhang, 2006; Tuch et al., 2001). Mac Donald et al have

☆ Diffusion tensor peripheral nerve tractography.

* Corresponding author. Fax: +81 3 3357 5445.
E-mail address: hidokano@sc.itc.keio.ac.jp (H. Okano).

1053-8119/$ – see front matter © 2008 Elsevier Inc. All rights reserved.
doi:10.1016/j.neuroimage.2008.09.022

obtained results indicating that DTI may be more sensitive than conventional MRI for evaluating traumatic brain injury (Mac Donald et al., 2007b).

Recent advances in MRI technology have made it possible to delineate peripheral nerve tracts in humans (Hiltunen et al., 2005; Meek et al., 2006; Skorpil et al., 2004). However, the reliability of DTT imaging has not yet been validated with detailed histological studies and quantitative analyses, so it has remained unclear whether the changes in DTT parameters actually correspond to the anatomical degeneration and regeneration of axonal fibers. Although the disintegration of axonal structures and demyelination occurring after peripheral nerve injury, known as Wallerian degeneration, is known to reduce the anisotropy of peripheral nerves (Beaulieu et al., 1996; Stanisz et al., 2001), and DTI has been shown to be useful for detecting axonal injury after traumatic brain injury (Mac Donald et al., 2007a,b) and ischemic injury of the optic nerve (Song et al., 2003; Sun et al., 2008), peripheral nerve tracking during the process of Wallerian degeneration has never been reported. We believe that since no proper tools are presently available for the visualization of peripheral nerves, it is important to evaluate the validity of applying DTT to assess peripheral nerve degeneration and regeneration. The objectives of the present study were to determine whether DTT is useful for tracking peripheral nerves, and to determine the relevance of the tracking parameters for evaluating fibers after peripheral nerve injury, by comparing them with histological and functional parameters of recovery.

Materials and methods

Animals and surgical procedures

One hundred twenty adult female Sprague-Dawley rats (165–228 g, 7 or 8 weeks of age; Clea Japan Inc., Tokyo, Japan) were used. All interventions and animal care procedures were performed in accordance with the Laboratory Animal Welfare Act, the Guide for the Care and Use of Laboratory Animals (National Institutes of Health), and the Guidelines and Policies for Animal Surgery provided by the Animal Study Committee of Keio University, and were approved by the Ethics Committee of Keio University. All surgeries were performed under chloral hydrate anesthesia (intraperitoneal injection; 350 mg per kg body weight; Wako Pure Chemicals, Osaka, Japan). The animals were housed in groups under a 12-hour light/dark cycle, with access to food and water *ad libitum*. The sciatic nerve was exposed through a dorsal gluteal muscle-splitting approach. The nerve was then subjected to a contusive injury at the sciatic notch using a brain aneurysm clip (Sugita clip; Mizuho Ikakogyo, Tokyo, Japan). The clip was closed and left in place for 5 min with a holding force of approximately 150 g (Kato et al., 2005).

Magnetic resonance imaging

MRI was performed using a 7.0-Tesla magnet (PharmaScan 70/16; Bruker BioSpin, Ettlingen, Germany) with a 38-mm volume coil dedicated for examinations of small animals. In studies using excised sciatic nerve, intact (pre-injured) excised nerves and nerves that had been excised 3 h, 1 day, 4 days, and 1, 2, 3, 4, 6, 8, and 12 weeks after the crush injury ($n=10$ each) were embedded in 2% agarose gel with 5 mM copper sulfate, and immediately subjected to diffusion tensor MRI. DTI data sets were acquired with a spin-echo sequence based on the Stejskal-Tanner diffusion preparation (Stejskal and Tanner, 1965). The scanning parameters were as follows: repetition time (TR), 15,000 ms; echo time (TE), 40 ms; flip angle, 90°; field of view (FOV), 40×40 mm; acquisition data matrix, 128×128; reconstructed image resolution, 0.31 mm; slice thickness, 0.94 mm; number of excitations (NEX), 1; b-value, 1000 s/mm^2; and motion probing gradient (MPG) orientations, 12 axes. Table 1 shows our normalized diffusion gradient orientations; duration of diffusion gradient pulses, 7 ms; diffusion time, 14 ms. The total imaging time was 6 h, 56 min.

Table 1
Normalized diffusion gradient orientations

Image volume	Gradients		
	x	*y*	*z*
1	0.0000	0.0000	0.0000
2	0.8944	0.0000	0.4472
3	0.0000	0.4472	0.8944
4	0.4472	0.8944	0.0000
5	0.8944	0.4472	0.0000
6	0.0000	0.8944	0.4472
7	0.4472	0.0000	0.8944
8	0.8944	0.0000	−0.4472
9	0.0000	−0.4472	0.8944
10	−0.4472	0.8944	0.0000
11	0.8944	−0.4472	0.0000
12	0.0000	0.8944	−0.4472
13	−0.4472	0.0000	0.8944

Diffusion tensor analysis

Diffusion tensor tractographic images were computed using the Volume One and dTV II SR software (Masutani et al., 2003). The diffusion tensor can be represented as an ellipsoid, where a proton at the center of the voxel has an equal probability of diffusing to any point in that ellipsoid. The eigenvectors of the diffusion tensor represent the three axes of the ellipsoid, namely, the length of the longest, middle, and shortest axes (called eigenvalues λ_1, λ_2 and λ_3). The eigenvector (e_1) associated with the largest eigenvalue (λ_1) was assumed to represent the local fiber direction. Fiber tracking was initiated from a manually selected region of interest (ROI), from which tracking lines were propagated bidirectionally according to the principal eigenvector (e_1) in each voxel. For the tractography, the ROI was placed at a site 5 mm proximal to the lesion epicenter, and the direction of the diffusion anisotropy was followed until the tracking was terminated at a voxel, depending on the threshold selected, with a fractional anisotropy (FA) of less than 0.25, 0.3, 0.4, 0.5, 0.6, 0.7, or 0.75. The FA value, a convenient index because it is scaled from 0 (isotropic) to 1 (anisotropic) (Mori and Zhang, 2006), can be calculated from the degree of diffusion anisotropy (Pierpaoli and Basser, 1996).

We determined the FA values and three eigenvalues (λ_1, λ_2, and λ_3) in each specimen at points 5 mm (proximal site), 0 mm (lesion epicenter), and −5 mm (distal site) from the lesion epicenter.

Histological analysis

Toluidine blue staining (light microscopy)

Samples were fixed in 2.5% glutaraldehyde/0.1 M cacodylate buffer (pH 7.4) for 12 h, then washed in cacodylate buffer, post-fixed for 2 h in 1% OsO_4/0.1 M cacodylate buffer (pH 7.4), dehydrated in a graded alcohol series and acetone, and finally embedded in epoxy resin. Semi-thin sections (1 μm thick) were cut cross-sectionally from the injured nerve specimens from a site 5 mm distal to the lesion epicenter and at the lesion epicenter at 4 days, 3 weeks, and 12 weeks after the crush injury, and stained with toluidine blue (1%) for 20 min; the corresponding sections from intact nerve specimens were also examined. The stained sections were then examined under a light microscope (AxioCam 2; Carl Zeiss, Jena, Germany).

Uranyl acetate staining (electron microscopy)

Ultrathin sections (80 nm thick) were obtained from the intact and injured nerve specimens at the same sites and time points as for the light microscopic examination, and stained with uranyl acetate (4.7%) for 30 min and Reynold's lead citrate for 8 min. Micrographs from 20 random fields of 17×17 μm^2 were obtained under a transmission

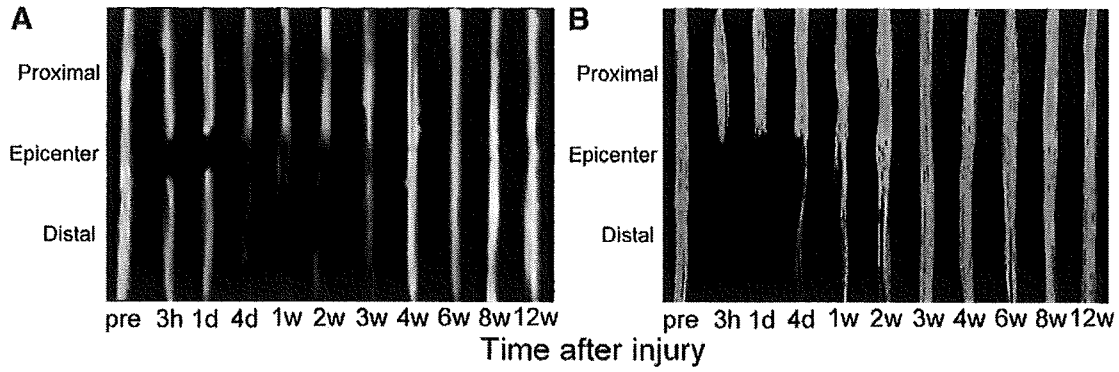

Fig. 1. FA map (A) and diffusion tensor tractography (B) of intact and injured sciatic nerves. For the tractography, the region of interest (ROI) was placed 5 mm proximal to the lesion epicenter. The FA value threshold was set at 0.4. In the DTT image constructed using this FA threshold value, the recovery process of the contused peripheral nerves could be clearly detected under the imaging parameters used.

electron microscope (JEOL model 1230; JEOL Ltd., Tokyo, Japan), by Digital Micrograph 3.3 (Gatan Inc., Warrendale, Pennsylvania, USA).

Quantitative analysis

Nerve samples were obtained at each of the ten time points used for diffusion tensor analysis, and subjected to quantitative determinations at the distal site, at which Wallerian degeneration/regeneration occurred. The following parameters were calculated for each nerve using the MCID system (Imaging Research, Inc., Toronto, Ontario, Canada): axon density, axon diameter, myelin sheath density, and myelin sheath thickness. Axon density was defined as axonal area/ total area, and myelin sheath density was defined as myelin sheath area/ total area in a fascicle in each nerve sample. The axon diameter and myelin sheath thickness of 40 randomly selected axons were

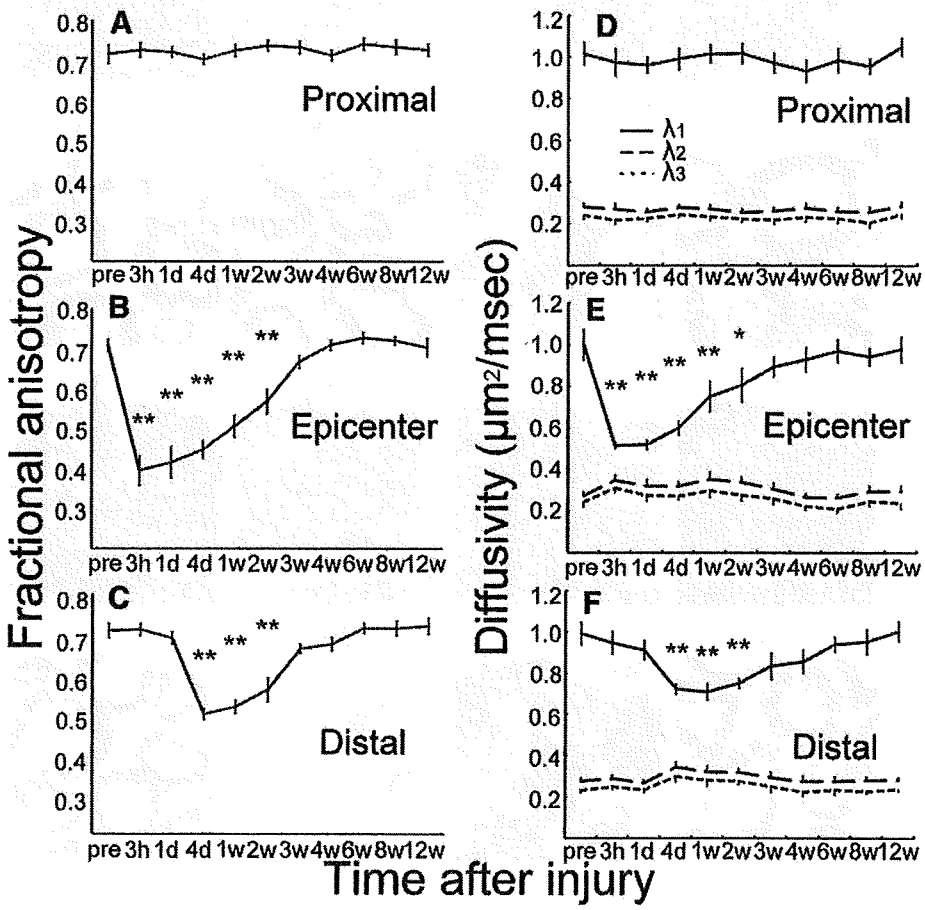

Fig. 2. Quantitative and temporal analysis of the FA values (A, proximal site; B, epicenter site; C, distal site), and eigenvalues (D, proximal site; E, epicenter site; F, distal site) ($n=10$ each). At the lesion epicenter, the FA value decreased sharply at 3 h and recovered gradually, reaching the pre-injury level by 3 weeks after the injury (B). At the distal site, while no significant change in the FA value was observed at 3 h or 1 day after the injury, a decrease was observed at 4 days, with gradual recovery thereafter to the pre-injury level by 3 weeks after the injury (C). The present model showed that both λ_2 and λ_3 were more constant than λ_1 (D–F), and that changes in FA values during the recovery after peripheral nerve injury depended mainly on λ_1, which represents the diffusivity along the longitudinal axis of the nerve. Statistical significance was determined to be $P<0.05$ using Dunnett's multiple comparison. Data represent the mean±SEM. *$P<0.05$; **$P<0.01$.

measured in each nerve sample. We also examined the changes in the distribution of the axon diameter after injury.

Behavioral analysis

Three different tests were used to assess the functional recovery after sciatic nerve injury. Ten rats were used for each functional evaluation. Each rat was examined at the same time-points used for the diffusion tensor analysis.

Leg muscle contraction test

The motor function of the lower extremities of the animals was evaluated using the leg muscle contraction test, in which isometric plantar flexion at the ankle is tested by pushing the sole until the toe touches the knee. A digital force gauge (Nidec-Shimpo Corp., Kyoto, Japan) was used for this test. The ratio of the degree of muscle contraction on the injured side to that on the contralateral sham-operated side was averaged.

Rota-rod test

The motor coordination of the animals was assessed using a rotating rod apparatus (Muromachi Kikai Co., Ltd., Tokyo, Japan) consisting of a plastic rod (9 cm in diameter) with a gritted surface, flanked by two large discs (50 cm in diameter) to prevent interference from other animals, at a height of 20 cm from the floor. The experimental rat was placed on the rod, and the rod was rotated at a speed of 15 rpm, following acclimation sessions (3 trials each at 5 and 10 rpm). The latency period until the rats fell off the apparatus was monitored for 180 s.

von Frey filament test

The mechanical sensitivity, which is the capacity of a sense organ to respond to mechanical stimulation, of the animals was tested using von Frey filaments (North Coast Medical Inc., Morgan Hill, California, USA) with calibrated bending forces (Tamae et al., 2005). Rats were placed individually in an acrylic cap (12 cm in diameter, 7 cm in height, and weighing 256 g) with a wire mesh bottom. After the rats

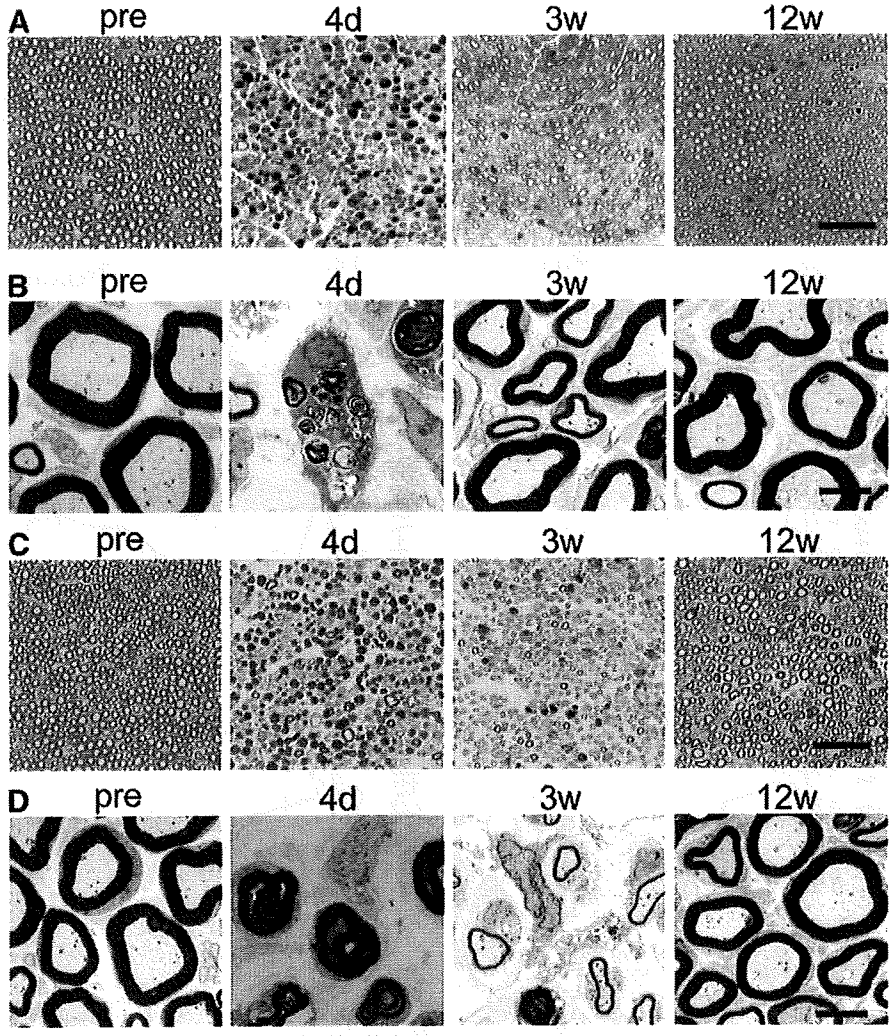

Fig. 3. Histological changes in the peripheral nerves at the lesion epicenter and at the distal site. Sections of 1 μm (A), stained with toluidine blue, and 80 nm (B), stained with uranyl acetate, were obtained from the lesion epicenter. Loss of axons and myelin debris arising from demyelination were observed 4 days after the injury (A). The phagocytosis of myelin debris by macrophages was observed (B). At 3 weeks after the injury, as the amount of myelin debris and number of macrophages decreased, myelinated axons became prominent. At 12 weeks after the injury, a similar number of myelinated axons to that in the pre-injury sciatic nerve was observed (A, B). Sections of 1 μm (C) stained with toluidine blue, and 80 nm (D) stained with uranyl acetate, were obtained from the site distal to the lesion epicenter. The series indicates that the axonal structures began to disintegrate within 4 days after the injury, then the axons began to regenerate by 3 weeks after the injury, and reached almost the pre-injury level of maturity by the end of the experimental period (C). Myelin debris was frequently detected 4 days after the injury. Macrophage recruitment, presumably for phagocytosis of the myelin debris, and very small axons within thin myelin sheaths were observed 3 weeks after the injury, followed by the formation of myelinated axons (D). (AX, axon; MS, myelin sheath; SC, Schwann cell; M, macrophage; scale bar, (A, C) 50 μm, (B, D) 5 μm).

had adapted to the testing environment for 60 min, the von Frey filaments were pressed perpendicularly against the plantar skin and held for 3–5 s with the filaments slightly buckled. Lifting of the paw was recorded as a positive response. The filaments were applied to the point of bending, six times each, to the plantar surface of the left and right hind paw, i.e., for a total of 12 times per rat, at intervals of 5 s; the next lightest filament was chosen for each subsequent measurement. The paw withdrawal threshold was taken as the lowest force that caused 100% withdrawals, and was considered the mechanical nociceptive threshold. The threshold ratio of the contralateral sham-operated side to that of the injured side was averaged.

Statistical analysis

All values were presented as the mean ± standard error of the mean (SEM). Statistical significance was determined as $P<0.05$ using Dunnett's multiple comparison. Pearson's correlation coefficients were calculated to determine the correlations between the histological/functional parameters and the diffusion imaging parameters. The SPSS statistical analysis software (version 16.0) was used for the analyses (SPSS Japan Inc., Tokyo, Japan).

Results

Diffusion tensor tractography and fractional anisotropy of injured peripheral nerves

We generated FA maps and delineated DTT images of the rat sciatic nerve for 12 weeks after contusive injury. On the FA maps (Fig. 1A), a sharp decrease in the intensity at the lesion epicenter was noted 3 h after the injury; thereafter, the intensity recovered gradually, reaching the pre-injury level by 4 weeks after the injury. At the distal site, the intensity was still preserved at both 3 h and 1 day; however, it was significantly decreased 4 days after the injury, and recovered gradually thereafter, reaching pre-injury levels by 4 weeks after the injury. Since tracking of the sciatic nerve depends on the selected FA threshold, at which the tracking is stopped, we also delineated DTT images of the sciatic nerves for 12 weeks after the injury using different FA thresholds: 0.25, 0.3, 0.4, 0.5, 0.6, 0.7, or 0.75 (Supplementary Figs. 1A–G). We found that the DTT images obtained using a FA threshold value of 0.4 (Fig. 1B) clearly showed the recovery process of the contused nerves. At 3 h after the injury, the fibers from the designated proximal site could not be tracked beyond the lesion epicenter, and fiber tracking could not proceed beyond the lesion epicenter until 1 day after the injury. On the other hand, a few fibers could be tracked distally by 4 days after the injury. The tractography revealed a return of the tracking parameters to the pre-injury levels, close those of the normal sciatic nerve, by 3 weeks after the injury.

To analyze the changes in the anisotropy of the injured sciatic nerves by DTI, we measured the FA values for 12 weeks after the injury. There were no significant changes in the FA value at the proximal site at any time point examined (Fig. 2A). In contrast, at the lesion epicenter, a sharp decrease in the FA value was observed 3 h after the injury, which then recovered gradually, reaching the pre-injury level by 3 weeks after the injury (Fig. 2B). In the images of the distal site, while no significant change in the FA value was observed at 3 h or 1 day, a decrease in the FA value was observed at 4 days, followed by gradual recovery thereafter, to the pre-injury level by 3 weeks after the injury (Fig. 2C).

We next analyzed the individual eigenvalues. The first eigenvalue (λ_1), which represents the diffusivity along the longitudinal axis of the nerve, was substantially higher than the second (λ_2) and third (λ_3) eigenvalues, which represent the diffusivity in directions perpendicular to the longitudinal axis. These radial diffusivities (λ_2 and λ_3) were much lower than the diffusivity value along the axis of the tract (λ_1). Thus, the present model showed that both λ_2 and λ_3 were more constant than λ_1 (Figs. 2D–F), and that the changes in the FA values after peripheral nerve injury depended mainly on λ_1, which represents the diffusivity along the longitudinal axis of the nerve.

Table 2
Correlations of the diffusion imaging parameters (Pearson's *r*) with the histological parameters

	Axon density	Axon diameter	Myelin density	Myelin thickness
FA	0.8618****	0.9166****	0.2387	−0.6941*
λ_1	0.9605****	0.9607****	0.4449	−0.5780

* $P<0.05$.
**** $P<0.001$.

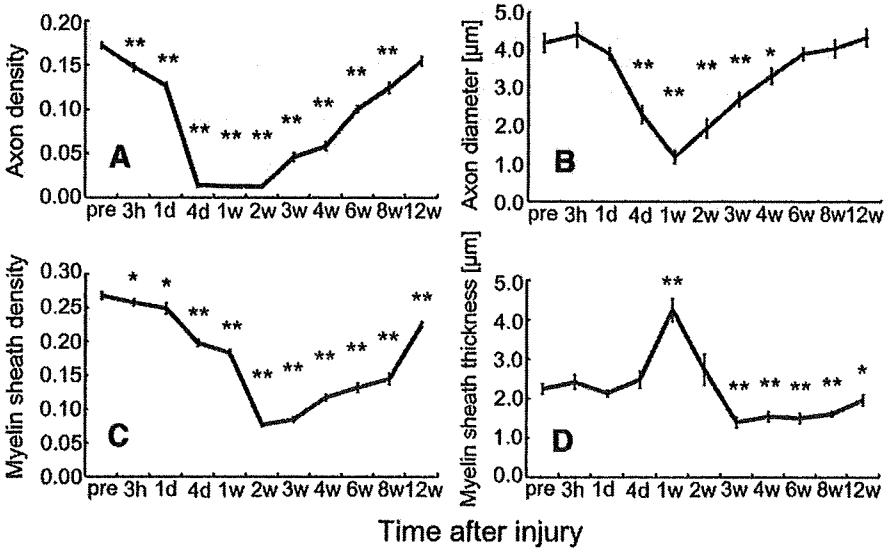

Fig. 4. Quantitative and temporal analysis of the axon density (myelinated axon area / total sectioned nerve area) (A), axon diameter (B), myelin sheath density (myelin sheath area / total sectioned nerve area) (C), and myelin sheath thickness (D) at the nerve site distal to the lesion epicenter ($n=10$ each). Statistical significance was determined to be $P<0.05$ using Dunnett's multiple comparison. Data represent the mean±SEM. *$P<0.05$; **$P<0.01$.

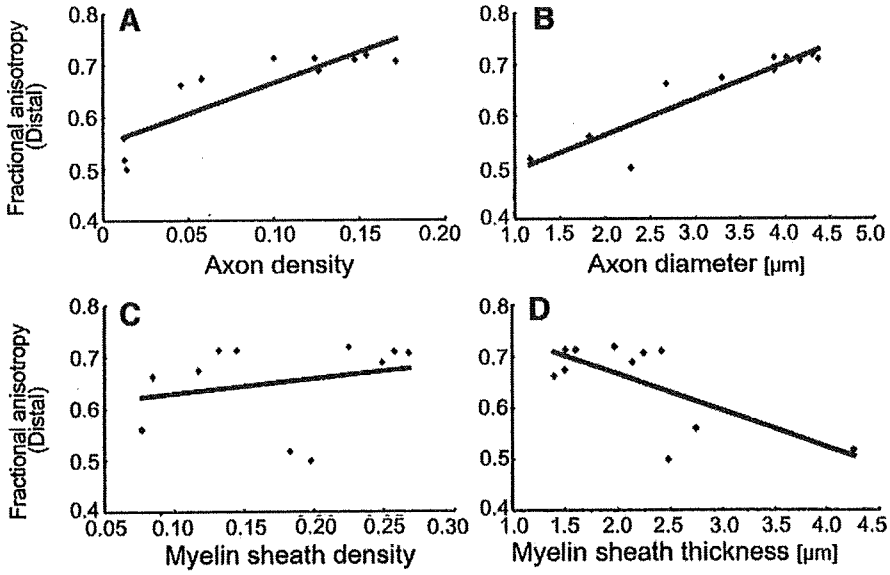

Fig. 5. Correlations between FA values and histological parameters. The FA values at the distal site were strongly correlated with each of the axonal parameters (A, Axon density, r=0.8618, P=0.0006; B, Axon diameter, r=0.9166, P=0.0001; C, Myelin sheath density, r=0.2387, P=0.4796; D, Myelin sheath thickness, r=−0.6941, P=0.0178).

Histological changes in the injured peripheral nerves

To examine the histological changes in the axons and myelin sheaths in detail, we performed toluidine blue and uranyl acetate staining of the nerves at the lesion epicenter and the distal site. At the lesion epicenter, axon loss and myelin debris arising from demyelination were observed 4 days after the injury (Fig. 3A). Consistent with these findings, EM examination revealed myelin debris being phagocytosed by macrophages (Fig. 3B). Subsequently, 3 weeks after the injury, as the amount of myelin debris and number of macrophages decreased, and myelinated axons began to appear prominently. At 12 weeks after the injury, myelinated axons similar in appearance and number to those in the pre-injury sciatic nerve were observed (Figs. 3A and B). At the distal site 4 days after the injury, more myelin debris and greater irregularity of the myelin sheaths were observed compared with the lesion epicenter (Figs. 3C and D), and fewer phagocytic macrophages were detected than at the lesion epicenter. A few regenerating axons, which appeared to be myelinated axons of smaller caliber with a thinner myelin sheath compared to normal axons, could be detected at 3 weeks, and these axons gradually reached the pre-injury level of maturity by 12 weeks after the injury (Fig. 3C). Three weeks after the injury, there was still a little myelin debris, which was being phagocytosed by macrophages, and a few small axons with thin myelin sheaths. These immature myelinated axons became progressively more mature and prominent with a thick myelin sheath, and the regenerated axons appeared similar to the axons observed pre-injury, by 12 weeks after the injury (Fig. 3D).

To analyze these changes quantitatively, we focused on the distal site, at which the Wallerian degeneration and regeneration could be clearly observed. We measured the number of axons, and the ratio of the myelinated axon area to the total sectioned nerve area as the axon density. The axon density decreased immediately after the nerve injury, reaching a minimum between 4 days and 2 weeks after the injury, and recovered gradually thereafter (Fig. 4A).

At this distal site, we also measured the ratio of the myelin sheath area to the total sectioned nerve area as the myelin sheath density. The myelin sheath density decreased gradually, reaching a minimum value 2 weeks after the injury, and began to recover thereafter (Fig. 4C). In addition, the axon diameter and myelin sheath thickness were measured in ultrathin (80 nm) sections under the electron microscope. No significant change in the axon diameter was noted until 1 day after the injury. Thereafter, with the swelling and degeneration of the myelin sheath, the axon diameter began to decrease, reaching a minimum at 1 week, and then recovered to the pre-injury level by 6 weeks after the injury (Fig. 4B). Furthermore, there was an obvious change in the pattern of axon diameter distribution pre and post injury (Supplementary Fig. 2). In contrast, the myelin sheath thickness increased to its maximum value at

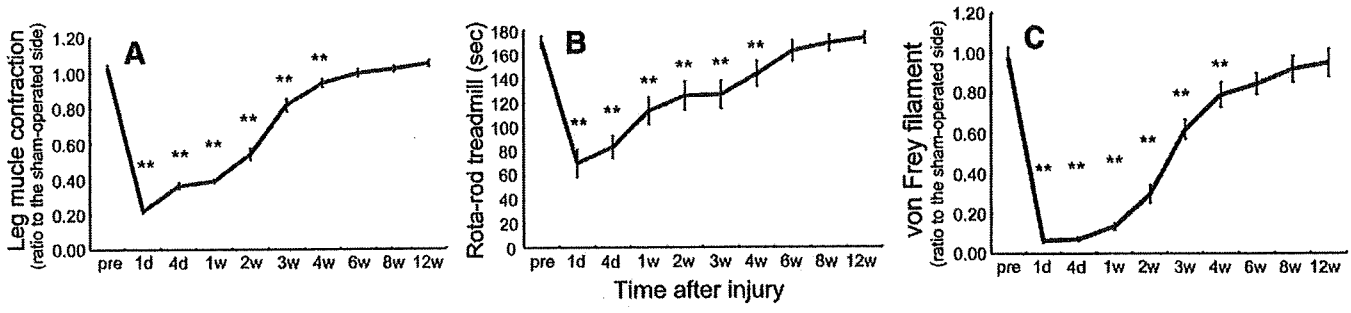

Fig. 6. Temporal analysis of the recovery of motor function in the lower extremities by the leg muscle contraction test (A), of motor coordination by the Rota-rod test (B), and of mechanical sensitivity by the von Frey filament test (C) for 12 weeks after contusion injury of the nerve. All three behavioral evaluations revealed functional recovery within 6 weeks of the nerve injury in this experimental model. Statistical significance was determined to be P<0.05 using Dunnett's multiple comparison. Data represent the mean±SEM. *P<0.05; **P<0.01.